A multi-grid finite-volume method for free-surface flows

Evangelia D. Farsirotou[1], Johannes V. Soulis[2]

[1]Department of Civil Engineering T.E., Faculty of Applied Sciences, Technological Educational Institute of Thessaly, 411 10 Larissa, Greece.

[2]Department of Civil Engineering, Fluid Mechanics/Hydraulics Division, Democritus University of Thrace, Xanthi 67100, Greece.

Abstract*—A depth-averaged subcritical and/or supercritical, steady, free-surface flow numerical model is developed to calculate physical hydraulic flow parameters in open channels. The vertically averaged free-surface flow equations are numerically solved using an explicit finite-volume numerical scheme in integral form. The grid used may be irregular and conforms to the physical boundaries of any problem. A multi-grid algorithm has been developed and has subsequently been applied to accelerate the convergence solution. A grid clustering technique is also applied. The numerical approach is straight forward and the flow boundary conditions are easy enforced. The capabilities of the proposed method are demonstrated by analyzing subcritical flow in an abrupt converging-diverging open channel flume as well calculating supercritical flows in an expansion channel. The computed results are satisfactorily compared with available measurements as well as with other numerical technique results. Very coarse grid gives satisfactory comparison results. The explicit numerical code can be utilized, within the assumptions made about the nature of the flow, for various vertically averaged free-surface flow calculations. Scope is to simulate free-surface flows of practical interest in a straight forward way. It can be extended to channel designs.*

Keywords*—*Multi-grid, Finite-volume, Subcritical-supercritical free-surface flow.

I. INTRODUCTION

In recent years significant advances have been made in computational fluid dynamics applied to free-surface flow calculations. The flow pattern of the aforementioned open channels either natural or technical is highly complex. There exist classes of free-surface flow problems, which can adequately be described in the context of depth-averaged 2D mathematical models. These simplified representations of 3D flows are justified where turbulent mixing, due to bottom roughness, effectively generates a uniform velocity distribution over the depth of the flow field. For free-surface flows in complex geometry it is convenient to make predictions using non-orthogonal boundary fitted computational meshes.

Numerous publications were reported for 2D free-surface flow simulation, among them Soulis J. [16] developed an explicit finite-volume numerical technique, with transformed grid, to simulate subcritical and supercritical depth-averaged free-surface flows. Molls T. et al. [8] derived a depth-averaged open channel flow model while Molls T. et al [9] applied an alternative direction implicit scheme and the MacCormack explicit scheme, both second order accurate, to numerically simulate 2D flows near spur-dikes. Yulistiyanto B. et al [19] solved the continuity and momentum equations for 2D horizontal flow by vertical depth-integration and the differential equations were also evaluated using the MacCormack scheme. Lien H. et al [6] presented a 2D depth-averaged model for simulating flow pattern in channel bends using an orthogonal curvilinear coordinate system to efficiently simulate the flow field with irregular boundaries. The two-step split-operator approach consisting of the dispersion step and the propagation step with the staggered grid was used to numerically solve the flow governing equations. Molls T. et al [10] numerically simulated supercritical flow in a channel with a wavy sidewall by solving the 2D depth-averaged equations using two different second-order accurate finite-difference schemes, an implicit model that uses an alternating direction implicit technique to solve the governing equations and an explicit model employing the MacCormack two-step predictor-corrector scheme. Liu M. et al [7] presented an unsteady 2D depth-averaged flow model to simulate the bend-flow field by transforming the governing system of differential equations into an equivalent system applied over a square-grid network in order to overcome the difficulties and inaccuracies associated with the determination of characteristics near the flow boundaries. The MacCormack two-step explicit scheme with second-order accuracy was used for the solution of the transformed system of equations. Papanicolaou A. et al [11] performed a sensitivity analysis to examine the predictive capability of a 2D hydrodynamic model, a finite-element surface water modeling system to adequately describe the flow characteristics around emergent bendway weir structures. Chen Y. et al [1] presented the water stage prediction-correction method, based on the theory of characteristics to couple numerical models in the boundary-connected way for shallow-water flows. An 1D–2D coupled numerical model was established, which incorporates the artificial porosity method capable of treating wetting and drying. Yu C. et al [17] proposed a surface flow routing algorithm

based on numerical solutions of shallow water equations and the kinematic wave approximation. The shallow water equations were discretized by the first-order Godunov-type finite-volume method. An implicit dual time-stepping method was applied by Yu H. et al [18] to a Godunov-type finite-volume model for 2D shallow-water flows on unstructured grids to improve run-time efficiency. In this model, an implicit nonlinear lower–upper symmetric Gauss–Seidel solution algorithm was used as an inner iteration solver for the implicit dual time-stepping method. Hu D. et al [4] developed a 2D finite-volume Eulerian-Lagrangian method on unstructured grid for solving the advection equation in free-surface scalar transport models.

The current numerical model was developed by Farsirotou E. [2], at the Department of Civil Engineering in Aristotle University of Thessaloniki, Greece. A 2D, viscous flow, finite-volume computational algorithm has been developed. An efficient and reliable multiple-grid algorithm has been applied to accelerate the convergence solution. The corrections to the fine-grid points are transferred to a coarse grid to maintain the low truncation errors associated with fine level of discretizations. Dense grid is incorporated wherever high gradient regions are encountered. Viscous flow stresses are described using either fixed value eddy viscosity coefficient or values related to the flow properties. Purpose of this research was, a) to develop a simple and easy to program algorithm without grid transformation, b) to achieve fast convergence multi-grid algorithm requiring minimal programming and c) to apply very coarse grid in achieving satisfactory comparisons with measurements. Scope is to simulate free-surface flows of practical interest in a straight forward way.

II. NUMERICAL MODEL

2.1 Theoretical assumptions

The channel flow is assumed to be homogeneous, incompressible and 2D with wind and Coriolis forces neglected. Hydrostatic pressure distribution is assumed throughout the flow field. The unsteady, free-surface flow in channels with fixed bed is described by non-linear, partial differential equations,

$$-\frac{\partial h}{\partial t}=\frac{\partial(hu)}{\partial x}+\frac{\partial(hv)}{\partial y} \tag{1}$$

$$-\frac{\partial(hu)}{\partial t}=\frac{\partial\left(gh^2/2+hu^2\right)}{\partial x}+\frac{\partial(huv)}{\partial y}-gh\left(S_{ox}-S_{fx}\right) \tag{2}$$

$$-\frac{\partial(hv)}{\partial t}=\frac{\partial\left(gh^2/2+hv^2\right)}{\partial y}+\frac{\partial(huv)}{\partial x}-gh\left(S_{oy}-S_{fy}\right) \tag{3}$$

x and y represent the Cartesian coordinate positions in the longitudinal and transverse directions respectively; t the time; u and v the average cross the depth velocity components in the x and y directions, respectively; h the water depth; g the gravity acceleration; $S_{0x}=-\partial z_b/\partial x$ and $S_{0y}=-\partial z_b/\partial y$ the channel slopes with $z_b$the bottom elevation above a datum and S_{fx} and S_{fy} the friction slopes defined, Kassem A. et al. [5], as,

$$S_{fx}=\frac{n^2u\sqrt{u^2+v^2}}{h^{4/3}} \text{ and } S_{fy}=\frac{n^2v\sqrt{u^2+v^2}}{h^{4/3}} \tag{4}$$

n is the Manning's flow friction coefficient. It is assumed that all of the resistance is due to bottom friction, thus neglecting the boundary layers on the side-walls, Molls T. et al. [8].

2.2 Application areas

Open channel flow problems, which can be adequately described in the context of depth-averaged, 2D mathematical models, where the flow properties can be assumed to be invariant along the vertical direction, are accurately simulated with the numerical model. The proposed program can be applied for free-surface determination in complex geometries with or without any obstructions into the flow region. Subcritical, supercritical or mixed subcritical-supercritical flows with automatic capturing of hydraulic jumps can also be simulated. In particular, the numerical code can be utilized for the calculation of:

- uniform flow using various flow friction coefficients,

- gradually varied flow as transitions, non-prismatic channels, backwater effects of dams etc,
- rapidly varied flow as parts of flow over spillways, hydraulic jumps in sloping channels, stilling basins, etc.

The code can be extended to, unsteady flows, morphology problems and channel designs.

III. NUMERICAL SIMULATION

3.1 Flow discretization

This program utilizes the finite-volume numerical method to solve the non-linear, parabolic, partial differential equations, Eqs. (1)-(3) in integral form, i.e. by applying the equations of continuity, x- and y-momentum to a series of finite-volumes with adjacent volumes sharing a common face, Farsirotou E. [2] and Soulis J. [16]. At the end of each time-step Δt the net flux into each elemental volume is zero, so that overall water mass flow is conserved, and the changes in momentum are equal to the forces imposed by the boundaries of the system. The 2D flow equations may be written down as conservation equations for a control volume ΔV of unit height and for a time step Δt as,

$$-\Delta h = \left[\Delta(hu)\Delta y + \Delta(hv)\Delta x\right]\frac{\Delta t}{\Delta x \Delta y} \tag{5}$$

$$-\Delta(hu) = \left[\Delta\left(gh^2/2 + hu^2\right)\Delta y + \Delta(huv)\Delta x\right]\frac{\Delta t}{\Delta x \Delta y} - gh\left(S_{ox} - S_{fx}\right)\Delta t \tag{6}$$

$$-\Delta(hv) = \left[\Delta\left(gh^2/2 + hv^2\right)\Delta x + \Delta(huv)\Delta y\right]\frac{\Delta t}{\Delta x \Delta y} - gh\left(S_{oy} - S_{fy}\right)\Delta t \tag{7}$$

The physical domain i.e. flow region is divided into polygonal sub-areas with quadrilateral form. These sub-areas are called finite-volumes of unit depth. The governing flow equations are solved in a non-transformed grid (physical grid). The solution attributes values for water depth h, axial u and tangential v velocities at each grid node. Application results into a series of arithmetic equations with nodal values of water depth, axial and tangential velocities as equation unknowns. Figure 1 shows the notation used for mass-flux balancing across a flow finite-volume. Similar notation is adopted for the balancing of x- and y-momentum. For ease application, all Δys are perpendicular to the x-axis. Thus, for water mass flux, an XFLUX is defined,

$$(\mathrm{XFLUX})_{i,j} = \left[\frac{(hu)_{i+1,j} + (hu)_{i,j}}{2}\right]\Delta y \tag{8}$$

The YFLUX is defined,

$$(\mathrm{YFLUX})_{i,j} = \left[\frac{(hv)_{i,j-1} + (hv)_{i,j}}{2}\right]\Delta x - \left[\frac{(hu)_{i,j-1} + (hu)_{i,j}}{2}\right]\Delta \mathrm{YB} \tag{9}$$

The second term comes from the mass fluxes balance into the ABE flow region, Fig.1.The ΔYB term is also defined in Fig. 1. The terms Δ(hu) and Δ(hv) of Eq. (5) are defined:

$$\Delta(hu) = (\mathrm{XFLUX})_{i,j} - (\mathrm{XFLUX})_{i,j-1} \tag{10}$$

$$\Delta(hv) = (\mathrm{YFLUX})_{i+1,j} - (\mathrm{YFLUX})_{i,j} \tag{11}$$

Similar differences are applied to all Δ terms, of Eqs. (6), (7). Thus, the water depth difference Δh in each i,j node of the involved finite-volume is calculated as,

$$\Delta h_{i,j} = \left[(\mathrm{XFLUX})_{i,j} - (\mathrm{XFLUX})_{i,j-1} + (\mathrm{YFLUX})_{i+1,j} - (\mathrm{YFLUX})_{i,j}\right]\frac{\Delta t}{\Delta x \Delta y} \tag{12}$$

Similar calculations are performed for the x-and y-momentum flux balancing. Backward differencing is used for the $\Delta/\Delta x$ estimation, while forward differencing is used for the $\Delta/\Delta y$ estimation. The slopes S_{ox} and S_{oy} are pre-calculated and stored

at the beginning of each time step, while the friction slopes S_{fx} and S_{fy} are continuously updated. For all bed and friction slopes, averaged values of the appropriate physical quantities are used.

3.2 Flow stabilization

The changes Δh, Δ(hu) and Δ(hv) are distributed between the four corners A, B, C and D of the finite-volume of Fig.1. However, this distribution affects the stability and the accuracy of the method. In the current research work it was decided to send 40.0% information regarding Δh change to the upstream face of the finite-volume, while the remaining 60.0% is sent to the downstream face. The Δ(hu) and Δ(hv) changes are taken as the averaged values of i and i-1 nodes of the computational grid. Also, and this is crucial in achieving convergence, the water depth value h is calculated taking into account the currently involved finite-volume depth and the one located at immediate downstream. The decision was made after numerical experimentation. All changes Δh, Δ(hu) and Δ(hv) were not directly used to yield the h, hu and hv values. For all test runs a C_1 factor is used for the h estimation and a C_2 for the (hu) and (hv) calculations,

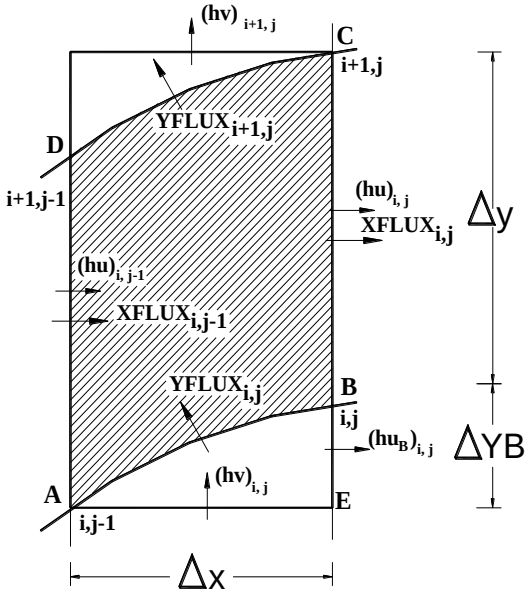

FIG. 1. NOTATION FOR THE MASS FLUX ACROSS A FINITE-VOLUME

$$h_{i,j}^{n+1} = h_{i,j}^{n} + \frac{\Delta h_{i,j}^{n+1}}{1 + \frac{C_1}{h^{0}_{1,1}} \Delta h_{i,j}^{n+1}} \tag{13}$$

$$(hu)_{i,j}^{n+1} = (hu)_{i,j}^{n} + \frac{\Delta(hu)_{i,j}^{n+1}}{1 + \frac{C_2}{(hu)^{0}_{1,1}} \Delta(hu)_{i,j}^{n+1}} \tag{14}$$

n is the iteration number. Similar expression holds for (hv) calculation. The above empirical coefficients numerically derived with typical values C_1=0.1 and C_2=0.025 are needed to stabilize the solution particularly during at the first Δt time-steps. These empirical values have minimal influence on the solution convergence after the first time-steps. The numerical scheme was found to be stable over a wide range of C_1 and C_2 values.

3.3 Multi-grid approach

The multi-grid algorithm described here consists of a fine-grid solution procedure and a coarse-grid acceleration scheme, Soulis J. [14]. In the current approach, the solution is advanced simultaneously on coarse and on fine-grid. Figure 2 shows a 2x2 multi-grid block. Thus, a coarse grid is formed grouping several finite-volumes into a block. The $\Delta h, \Delta(hu)$ and $\Delta(hv)$, changes, Eqs. (5)-(7), at the end of every time-step are known for each finite-volume of the fine-grid mesh. The

changes for the block can be found by summing the fluxes around its faces. Another way to find the changes for the block is to sum the already calculated changes for the finite-volume within the block.

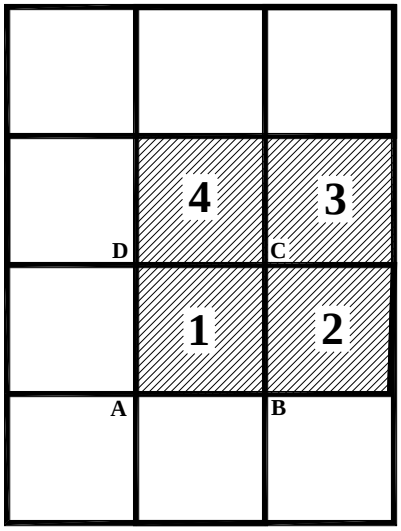

FIG. 2. A TYPICAL 2X2 MULTI-GRID

For a typical 2x2 block size application these changes are determined as follows,

$$\Delta h_{2x2} = \Delta h_1 + \Delta h_2 + \Delta h_3 + \Delta h_4 \tag{15}$$

subscripts 1,2,3,4 denote the mesh control volumes, Fig. 2. Similarly,

$$\Delta(hu)_{2x2} = \Delta(hu)_1 + \Delta(hu)_2 + \Delta(hu)_3 + \Delta(hu)_4 \tag{16}$$

$$\Delta(hv)_{2x2} = \Delta(hv)_1 + \Delta(hv)_2 + \Delta(hv)_3 + \Delta(hv)_4 \tag{17}$$

Thereafter, the flow properties changes at fine-grid points are calculated,

$$\Delta h_1^{new} = \Delta h_1 + I_{2x2}^{fine} \Delta h_{2x2} \tag{18}$$

$$\Delta(hu)_1^{new} = \Delta(hu)_1 + I_{2x2}^{fine} \Delta(hu)_{2x2} \tag{19}$$

$$\Delta(hv)_1^{new} = \Delta(hv)_1 + I_{2x2}^{fine} \Delta(hv)_{2x2} \tag{20}$$

I_{2x2}^{fine} is a linear interpolation operator. The calculations using Eqs. (18)-(20) are repeated for the remaining 2, 3 and 4 finite-volumes of the under consideration block. With the multiple grid application, the use of the blocks minimizes the computational work needed to propagate the unsteady waves out of the computational domain so that a steady-state solution is rapidly reached. The convergence of the multi-grid method is typically 3 times faster than a single grid. Figure 3 shows the convergence histories for supercritical type of flow calculation using various multi-block schemes. The 2x2 multi-grid block give the fastest convergence for current method applications.

3.4 Grid clustering

Computational grid formation requires minimum data. Grid nodes need not to be uniform in any direction. Flow problems with large gradients of the physical quantities need dense computational grid formation for efficient flow depiction. Then, rather using a uniform grid distribution in the tangential direction grid points may be clustered in high flow gradients regions. This reduces the total amount of required grid points.For a physical domain enclosed by lower and upper solid surfaces (channel flow) clustering at both surfaces may be considered. The following algebraic equation may be employed for this purpose, Hoffman K. et al. [3],

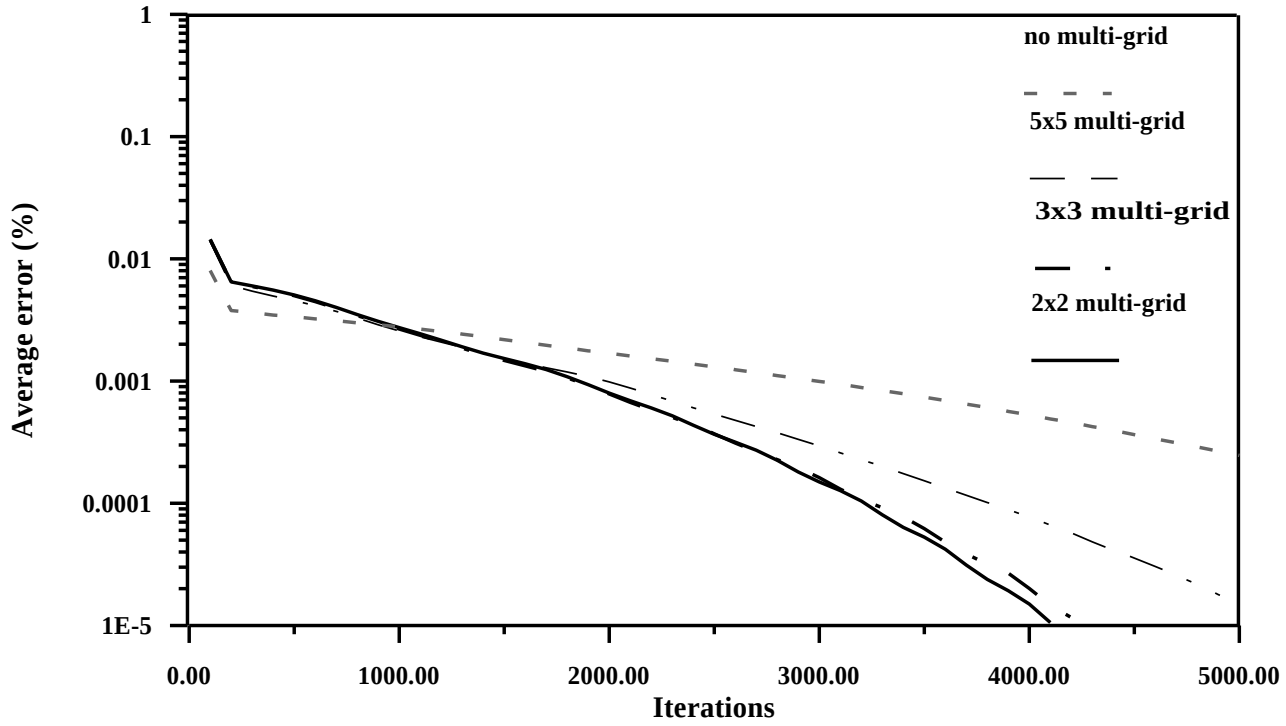

FIG. 3. CONVERGENCE HISTORY FOR THE ROUSE H. ET AL. (1951) EXPANSION CHANNEL USING VARIOUS MULTI-GRIDS

$$y(i,j) = y(1,j) + [y(IM,j) - y(1,j)]\frac{(2a+b)(BETA)^{ALFA} + 2a - b}{(2a+1)(1+BETA)^{ALFA}} \tag{21}$$

$$ALFA = \frac{\frac{i-1}{IM-1} - a}{1-a},\ BETA = \frac{b+1}{b-1} \tag{22}$$

IM is the maximum number of grid points in the transverse direction, b is a clustering parameter with values ranging from 1.05 for dense grid to 1.20 for less dense, while the factor a defines where the clustering takes place. Using a=0.0 clustering takes place at the upper wall while for a=0.5 clustering takes place at lower and upper wall.

3.5 Flow boundary conditions

There are two types of boundary conditions; the open boundaries and the solid boundaries. For subcritical flow entrance, at the upstream boundary a fixed value of the flow rate Q and a relative flow direction are specified. At the downstream boundary, a uniform across the width, water depth h is specified. For supercritical flow entrance, at the upstream boundary, the transverse flow velocity v component and a uniform across the width water depth h are specified along with total available head. At the downstream boundary all flow physical quantities left free to change. Simply, the physical quantity values are extrapolated from the interior grid nodes.

To close the problem, the condition of no water mass-flow across the solid boundaries needs to be applied (free-slip condition). This means that the velocity component normal to the solid face must be zero. This is easily achieved with the current grid formation and numerical discretization.

3.6 Numerical procedure

Firstly, geometrical and physical data describing the flow problem are read. Thereafter, the computational grid is formed. From the bed elevation the initial bottom slopes of the under examination channel are formed. A linear distribution of the $gh^2/2$ quantity between inlet and outlet flow boundaries is assumed and the u, v velocity components, as well as the water depth h are calculated. The iterations start by solving the water mass-flux Eq. (5) to obtain h^{n+1}, using old u^n, v^n and h^n and a corrected water depth is obtained. Then appropriate boundary flow conditions are applied at the inlet and outlet flow field.

Equations (6) and (7) are solved to obtain $(hu)^{n+1}$ and $(hv)^{n+1}$ and thereby new values for u^{n+1} and v^{n+1} are derived. Solid boundary conditions are applied requiring no water flow perpendicular to solid surface. Also, smoothing factors are applied to all changes of the flow field quantities. All changes are sent to the appropriate nodes of the finite-volume involved.

The convergence criterion requires that the averaged over the flow field relative error based on the axial velocity drops below $5x10^{-6}$. As with all time-marching methods the theoretical maximum stable time step Δt is specified according to the Courant-Friedrichs-Lewy (CFL) criterion,

$$\Delta t \le \left\{ \min\left(\frac{\Delta x}{u_{i,j} + \sqrt{gh_{i,j}}}, \frac{\Delta y}{v_{i,j} + \sqrt{gh_{i,j}}} \right) \right\} FT \tag{23}$$

Δx ($=x_{i,j}-x_{i,j-1}$) and Δy ($=y_{i+1,j}-y_{i,j}$) are the streamwise and transverse distances of a given finite-volume, respectively. The actually used values are calculated using the minimum of all Δxs and Δys of the grid. FT is a constant with less than unity value.

The described method is an explicit numerical technique requiring substantial computational time to achieve solution at the requested time level. The incorporation of the multi-grid approach ensures substantially faster convergence. The explicit formation is in favor of an implicit technique as far as the programming complexity is concerned. Programming the free-surface algorithm is straight forward process. The algorithm is written in a Fortran language.

IV. APPLICATIONS

4.1 2D subcritical flow in a converging-diverging channel

The reliability of the current model in subcritical flows is confirmed by comparing numerical results with available measurements conducted by Soulis J. et al. [15]. Schematic plan view geometry of the tested laboratory flume (spur dike) is shown in Fig. 4. This flume was used to validate the numerical model simulation in subcritical free-surface flow. The channel length and width are 2.5 m and 0.25 m, respectively. At an axial, from inlet, distance 0.5 m the channel converges with a contraction angle of 10.88^o. The convergence continues until the flume width reaches 0.125 m. The throat area extends 0.30 m. Thereafter, the lower side wall diverges with an expansion angle of 21.037^o until the width takes the value of 0.25 m.

For the numerical simulation a 48x11 (longitudinal x tangential) computational grid is used. The spatial step Δy is 0.025 m. However, the spatial step Δx for the converging part as well as for the throat region is 0.05 m while for the diverging part it is 0.025 m.The applied inflow discharge Q is 0.02606 m^3/s, while the downstream flow depth h is 0.284 m (subcritical flow conditions). The channel bottom slopes S_{0x} and S_{0y} are set zero. The Manning's flow friction coefficient n is estimated 0.012. Computational results of flow depth h and axial velocity magnitude u are presented along 3 different "streamlines". These are stream wise lines where measurements were taken at transverse distances of 0.05 m, 0.10 m and 0.20 m from the lower channel wall.

Comparisons between computed results and measurements, Soulis J. et al. [15], for the 0.05 "streamline" are shown in Fig. 5 for the water depth h and Fig. 6 for the u axial velocity magnitude. Axial velocities at the downstream end to the spur dike region were not available. Figures 7, 8, 9 and 10 show the water depth h and the axial velocity magnitude u for the 0.10 m and 0.20 m "streamlines' locations, respectively.

It is evident that the computed results agree rather well with the experimental measurements, particularly in the converging part of the channel. A discrepancy appears between measured and computed velocities in the diverging part of the channel, Fig. 10, where high viscous flow is developing. The tested spur dike obstacle constitutes a major difficulty from computational fluid dynamics point of view. Recirculating flow is present at the downstream spur dike end. However, the tested grid is sparse enough to adequately cover this highly turbulent region. The flow depths at the three "streamlines", both upstream and downstream from the converging part of the channel are also in good agreement with measurements and show the validity and practical reliability of the numerical model.

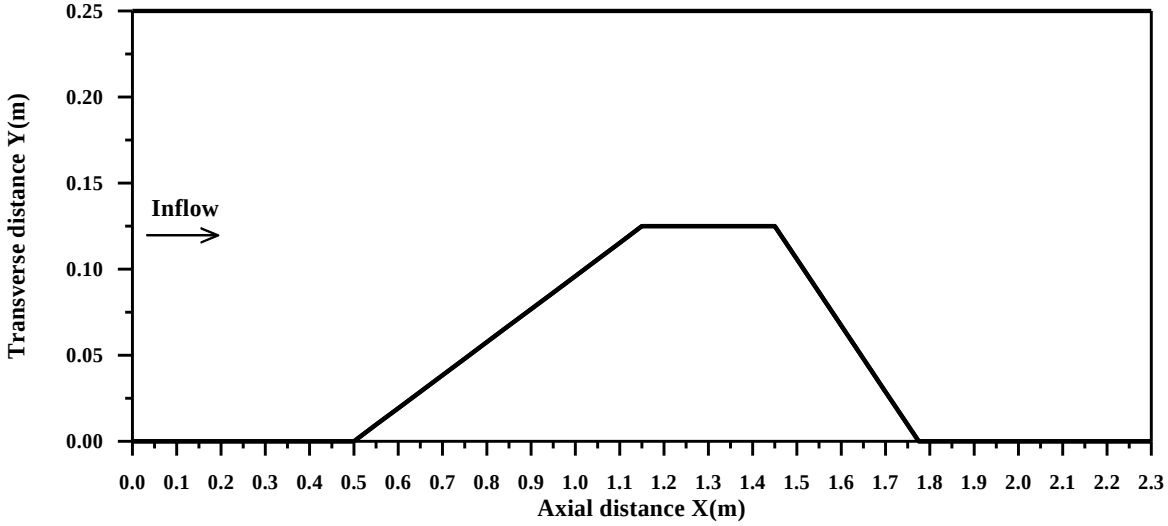

FIG. 4. CONVERGING- DIVERGING FLUME GEOMETRY

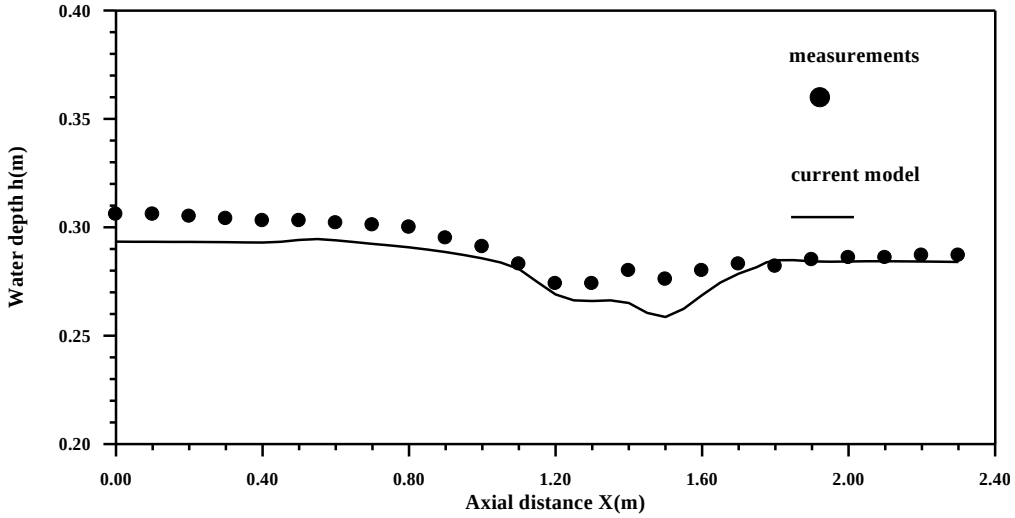

FIG. 5. WATER DEPTH COMPARISON BETWEEN CURRENT METHOD PREDICTIONS AND MEASUREMENTS ALONG A "STREAMLINE" LOCATED AT 0.05 M FROM LOWER WALL FOR THE CONVERGING-DIVERGING FLUME AT Q=0.02606 M^3/S

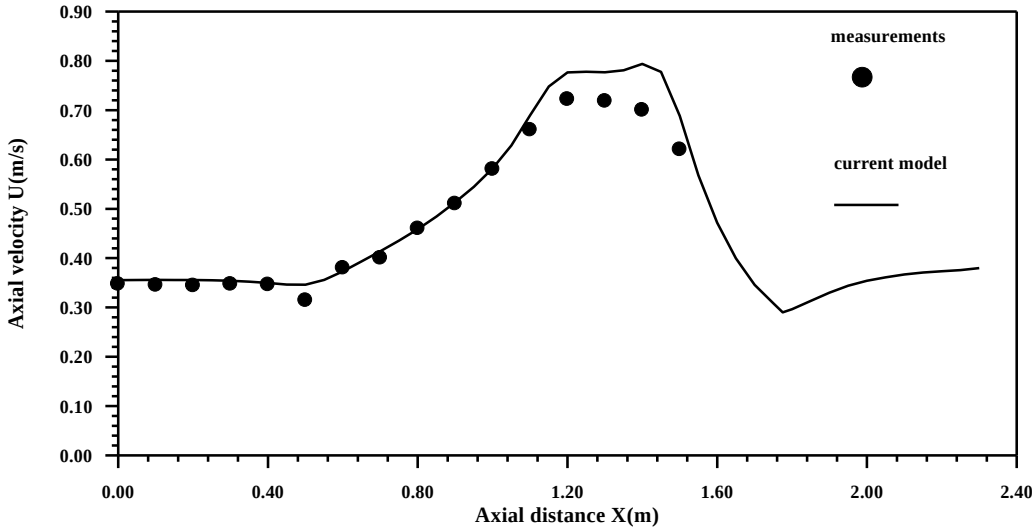

FIG. 6. AXIAL VELOCITY COMPARISON BETWEEN CURRENT METHOD PREDICTIONS AND MEASUREMENTS ALONG A "STREAMLINE" LOCATED AT 0.05 M FROM LOWER WALL FOR THE CONVERGING-DIVERGING FLUME AT Q=0.02606 M^3/S

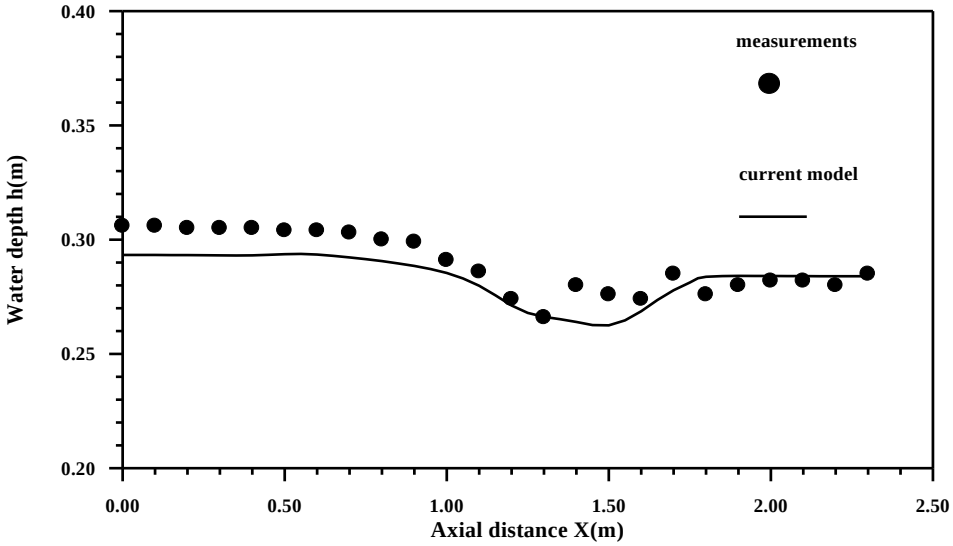

FIG.7. WATER DEPTH COMPARISON BETWEEN CURRENT METHOD PREDICTIONS AND MEASUREMENTS ALONG A "STREAMLINE" LOCATED AT 0.10 M FROM LOWER WALL FOR THE CONVERGING-DIVERGING FLUME AT Q=0.02606 M^3/S

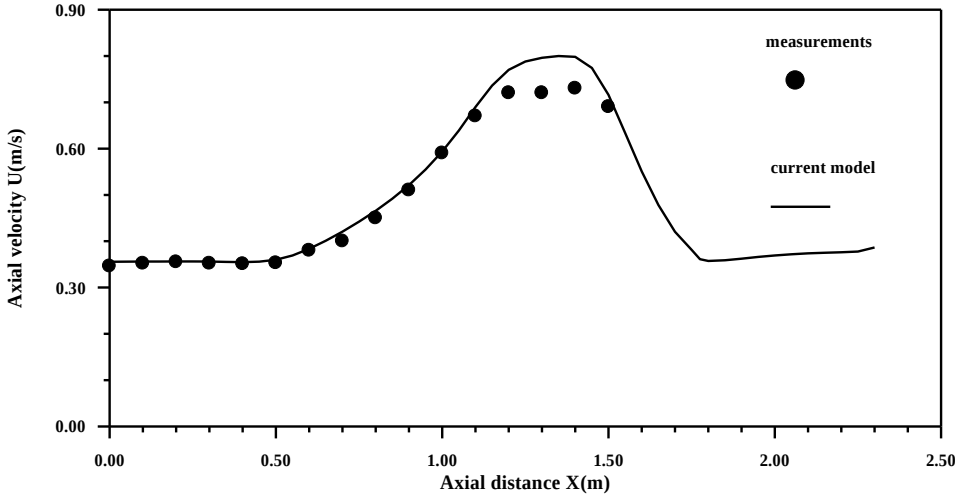

FIG. 8. AXIAL VELOCITY COMPARISON BETWEEN CURRENT METHOD PREDICTIONS AND MEASUREMENTS ALONG A "STREAMLINE" LOCATED AT 0.10 M FROM LOWER WALL FOR THE CONVERGING-DIVERGING FLUME AT Q=0.02606 M^3/S

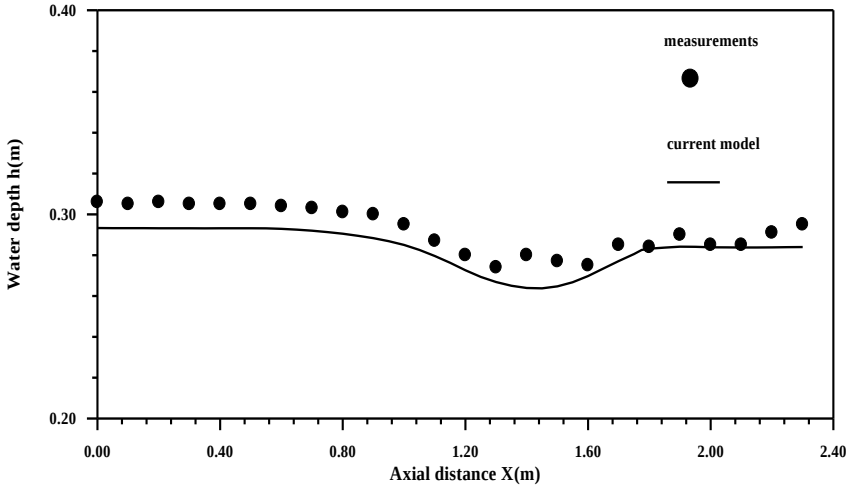

FIG. 9. WATER DEPTH COMPARISON BETWEEN CURRENT METHOD PREDICTIONS AND MEASUREMENTS ALONG A "STREAMLINE" LOCATED AT 0.20 M FROM LOWER WALL FOR THE CONVERGING-DIVERGING FLUME AT Q=0.02606 M^3/S

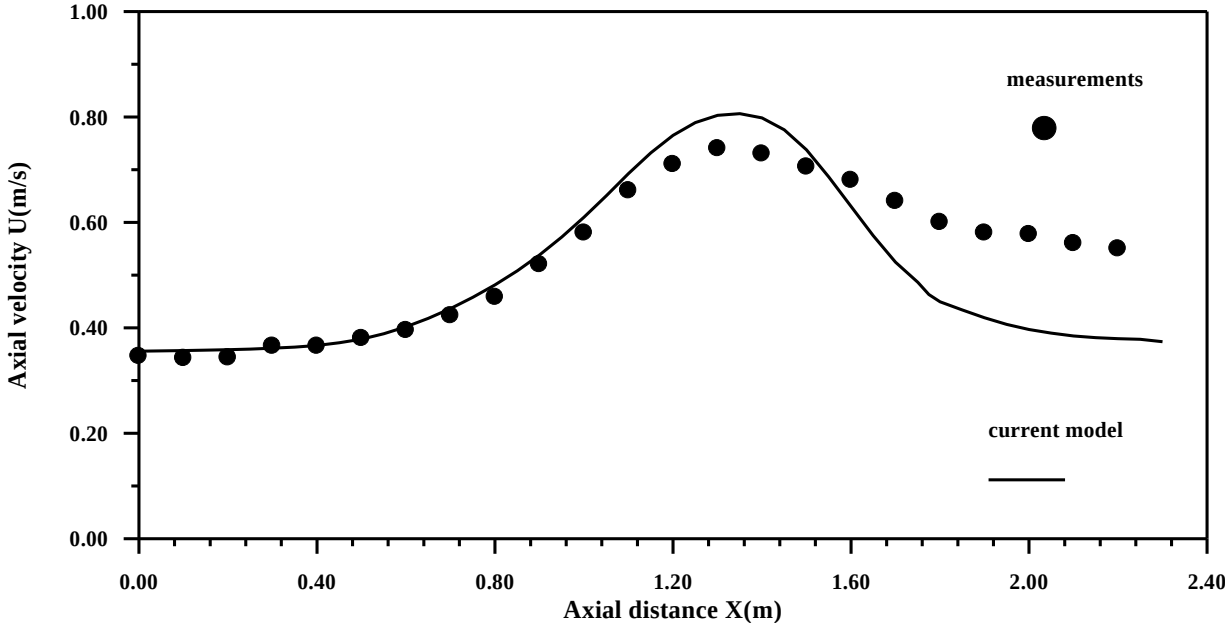

FIG. 10. AXIAL VELOCITY COMPARISON BETWEEN CURRENT METHOD PREDICTIONS AND MEASUREMENTS ALONG A "STREAMLINE" LOCATED AT 0.20 M FROM LOWER WALL FOR THE CONVERGING-DIVERGING FLUME AT Q=0.02606 M^3/S

4.2 2D supercritical flow in an expansion channel

The channel expansion, shown in Fig. 11, is used to test the accuracy of the proposed numerical method at high entrance Froude number of Fr_1=4.0. Rouse H. et al. [12] experimentally studied supercritical flow for the channel expansion. A 61x29 grid node is used for numerical simulation. The actual expansion channel geometry is described as,

$$\frac{y}{b_1} = \frac{1}{2}\left(\frac{x}{4.0b_1}\right)^{3/2} + \frac{1}{2} \tag{24}$$

b_1 is the half entrance width. At the upstream end, a constant value of water depth h_1 of 1.0 m is specified. A fixed value of the total available head 9.0 m is also specified. The Manning's roughness coefficient is 0.012.

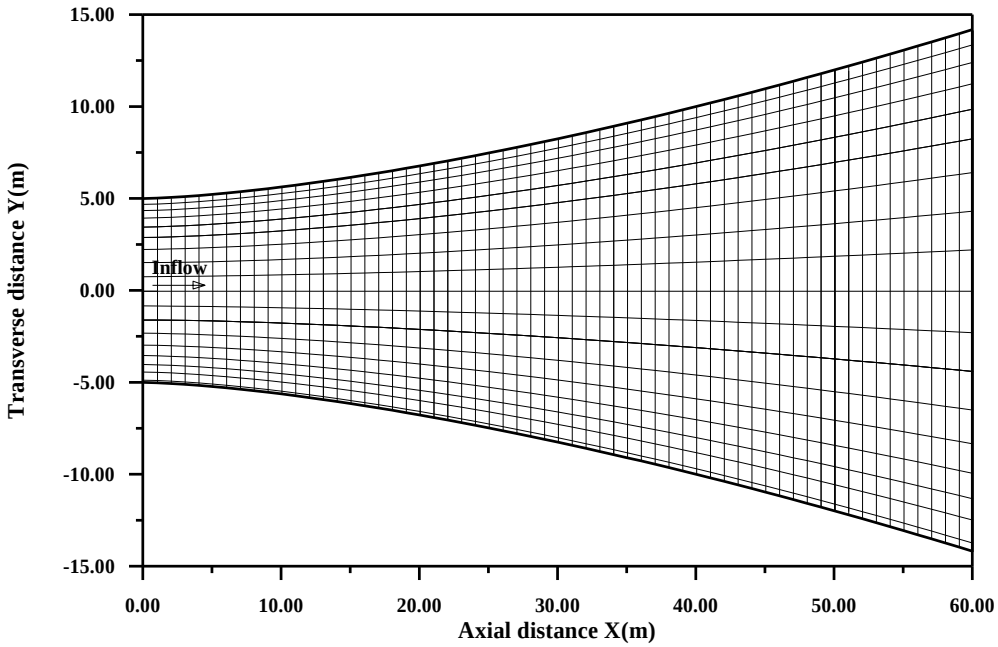

FIG. 11. EXPANSION CHANNEL GEOMETRY FOR FR1=4.0 AFTER ROUSE H. ET AL. (1951), CLUSTERED COMPUTATIONAL GRID

The current method computational results are compared with measurements,Rouse H. et al. [12] as well as with computational results using an explicit MacCormack numerical scheme, Soulis J. et al. [13]. Figures 12, 13 and 14 show the comparison for thecurved side, mid-stream line (line between axis of symmetry and curved side) and axis of symmetry, respectively. The current model comparison results with either measurements or with MacCormack's numerical method is considered to be satisfactory.It must be noted that the predicted results are closer to each other. The overall performance demonstrates that the proposed model is accurate and efficient for simulating free-surface flow in practical applications.

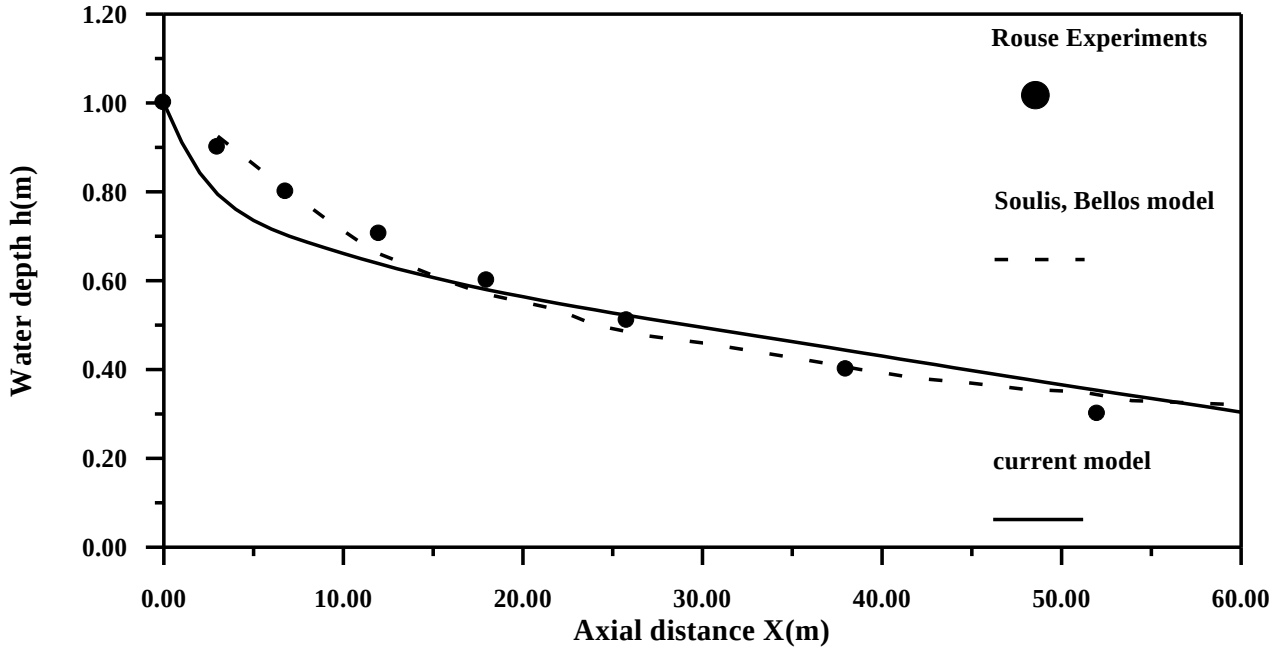

FIG. 12. WATER DEPTH COMPARISON BETWEEN CURRENT METHOD PREDICTIONS, MACCORMACK PREDICTIONS (SOULIS J. ET AL., 1989) AND MEASUREMENTS ALONG THE CURVED SIDEFOR THE ROUSE H. ET AL. (1951) CHANNEL AT FR1=4.0

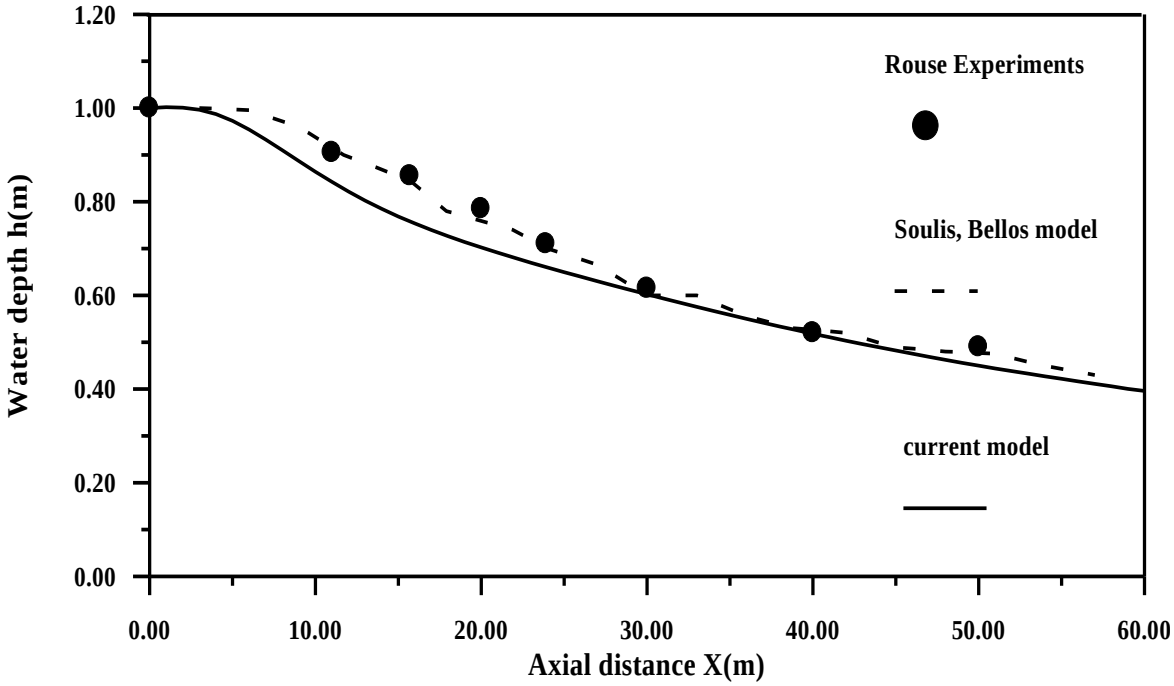

FIG. 13. WATER DEPTH COMPARISON BETWEEN CURRENT METHOD PREDICTIONS, MACCORMACK PREDICTIONS (SOULIS J. ET AL., 1989) AND MEASUREMENTS ALONG THE MID-STREAM LINE (LINE BETWEEN AXIS OF SYMMETRY AND CURVED SIDE) FOR THE ROUSE H. ET AL. (1951) CHANNEL AT FR1=4.0

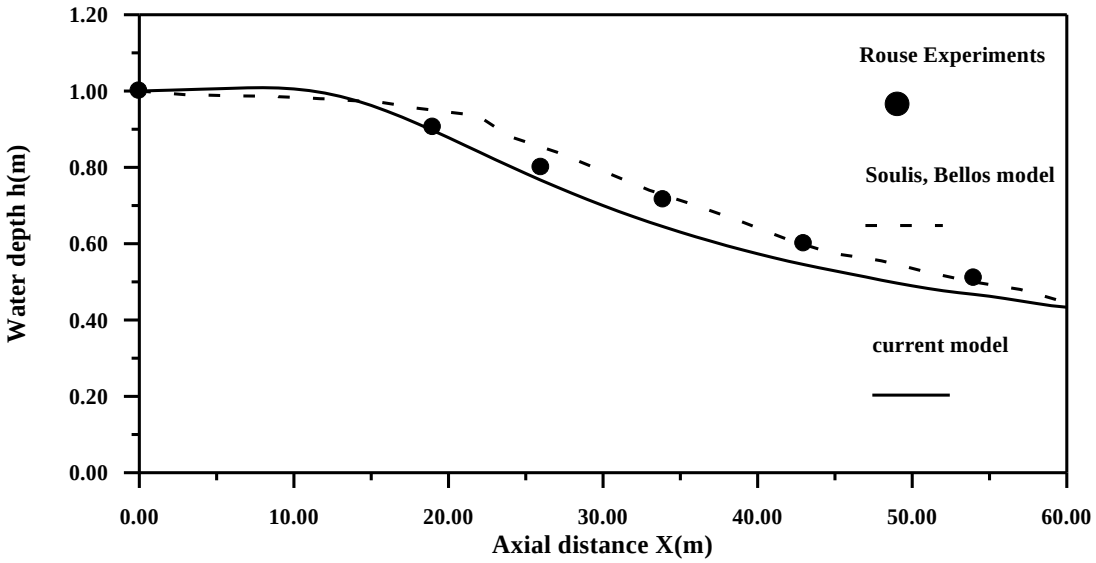

FIG. 14. WATER DEPTH COMPARISON BETWEEN CURRENT METHOD PREDICTIONS, MACCORMACK PREDICTIONS (SOULIS J. ET AL., 1989) AND MEASUREMENTS ALONG THE FLUME AXIS OF SYMMETRY FOR THE ROUSE H. ET AL. (1951) CHANNEL AT FR1=4.0

V. CONCLUSION

A depth-averaged, multi-grid, finite-volume, explicit, numerical scheme has been developed and subsequently applied to free-surface flow calculations. Main advantage of the proposed computational model is the ability to calculate subcritical and supercritical free-surface flow and to conform to physical boundaries of any open channel flow problem. The numerical approach is straight forward and the flow boundary conditions are easy enforced. The applied multi-grid acceleration technique gives very fast convergence. Application to a variety of open channel flow configurations is given to validate the method's potentialities. Applications regarding subcritical flow in a converging-diverging open channel and supercritical flow in a linearly expanding channel are reported. Comparisons with available measurements as well as with other numerical technique results show that the proposed method is a comparatively accurate and reliable technique. Very coarse grids give satisfactory comparison results. Free-surface flows simulation of practical interest in a straight forward way has been achieved. The method can be utilized for design computations.

REFERENCES

[1] Y. Chen, Z. Wang, Z. Liu and D. Zhu, (2012) "1D-2D Coupled Numerical Model for Shallow-Water Flows", Journal of Hydraulic Engineering", vol. 138, 2012, pp. 122-132.

[2] E. Farsirotou,"Numerical and experimental study of scouring in alluvial channels", Ph.D. Thesis, 2000, Aristotle University of Thessaloniki, Civil Engineering Department, Thessaloniki, Greece.

[3] K. Hoffmann and S. Chiang, "Computational Fluid dynamics for Engineers, 1993, Engineering Education System, Wichita, Kansas.

[4] D. Hu, Y. Zhu, D. Zhong and H. Qin, "Two-Dimensional Finite-Volume Eulerian-Lagrangian Method on Unstructured Grid for Solving Advective Transport of Passive Scalars in Free-Surface Flows", Journal of Hydraulic Engineering,vol. 143, 2017, 04017051.

[5] A. Kassem and M. Chaudhry, (1988) "Comparison of coupled and semi-coupled numerical models for alluvial channels", Journal of Hydraulic Engineering, ASCE, vol. 124, 1988, pp. 794-802.

[6] H. Lien, T. Hsieh, J. Yang andK. Yeh, "Bend-Flow Simulation 2D Depth-Averaged Model", Journal of Hydraulic Engineering, vol. 125, 1999, pp. 1097-1108.

[7] M. Liu, Y. Liu and W. Wei, "Numerical Simulation of 2D Flow in a Curved Channel", Advanced Materials Research, vol. 374-377, 2011, pp. 378-381.

[8] T. Molls and M. Chaudhry,"Depth-averaged open channel flow model", Journal of Hydraulic Engineering, ASCE, vol. 121, 1995, pp. 453-465.

[9] T. Molls, M. Chaudhry and K. Khan, "Numerical simulation of two-dimensional flow near a spur-dike", Advances in Water Resources, vol. 18, 1995, pp. 227-236.

[10] T. Molls and G. Zhao, "Depth-Averaged Simulation of Supercritical Flow in Channel with Wavy Sidewall", Journal of Hydraulic Engineering, vol. 126, 2000, pp. 437-445.

[11] A. Papanicolaou, M. Elhakeem and B. Wardman, (2011) "Calibration and Verification of a 2D Hydrodynamic Model for Simulating Flow around Emergent Bendway Weir Structures", Journal of Hydraulic Engineering, vol. 137, 2011, pp. 75-89.

[12] H. Rouse, B. Bhoota and En-Yen Hsu, "Design of channel expansions", Transactions ASCE, vol. 116, 1951, pp. 347-363.

[13] J. Soulis and K. Bellos, "Steady, supercritical, open channel flow computations", Proc. 6th International Conference on Numerical Methods in Laminar and Turbulent Flow, Swansea, U. K., 1989.

[14] J. Soulis J, "A Multi-grid method for open channel flow calculation", VIIIthInternational Conference on Computational Methods in Water Resources", Venice, Italy, 1990, pp. 221-230.

[15] J. Soulis, E. Alexiou and E. Kounavas, "Measurements and computations of non- uniform flow", TechnikaChronika-A, vol. 11,1991, pp. 59-82.

[16] J. Soulis, "A numerical method for subcritical and supercritical open channel flow", International Journal for Numerical Methods in Fluids, vol. 13, 1991, pp.437-464.

[17] C. Yu and J. Duan, (2014) "Two-Dimensional Hydrodynamic Model for Surface-Flow Routing", Journal of Hydraulic Engineering, vol. 140, 2014, 04014045

[18] H. Yu, G. Huang and C. Wu, "Efficient Finite-Volume Model for Shallow-Water Flows Using an Implicit Dual Time-Stepping Method", Journal of Hydraulic Engineering, vol. 141, 2015, 04015004

[19] B. Yulistiyanto, Y. Zech and W. Graf, "Flow around a Cylinder: Shallow-Water Modeling with Diffusion-Dispersion" Journal of Hydraulic Engineering, vol. 124(4),1998, pp.419-429.